Transition-State Structure for the ADP-Ribosylation of Recombinant $G_{i\alpha1}$ Subunits by Pertussis Toxin†

Johannes Scheuring,‡ Paul J. Berti, and Vern L. Schramm*

Department of Biochemistry, Albert Einstein College of Medicine, 1300 Morris Park Avenue, Bronx, New York 10461

Received October 20, 1997; Revised Manuscript Received December 11, 1997

ABSTRACT: Pertussis toxin ADP-ribosylates a specific Cys side chain in the α-subunit of several G-proteins. Recombinant $G_{i\alpha1}$-subunits were rapidly ADP-ribosylated in the absence of $\beta\gamma$-subunits, with a K_m of 800 μM and a k_{cat} of 40 min^{-1}. Addition of $\beta\gamma$-subunits decreases K_m to 0.3 μM with little change of k_{cat}. Kinetic isotope effects established the transition-state structure for ADP-ribosylation of $G_{i\alpha1}$ subunits. The transition state is dissociative, with a 2.1 Å bond to the nicotinamide leaving group and a bond of 2.5 Å to the sulfur nucleophile. The nucleophilic participation of $G_{i\alpha1}$ at the transition state is greater than that for water in the hydrolysis of NAD^+ by pertussis toxin. Crystal structures for $G_{i\alpha1}$ show the Cys nucleophile in a disordered segment or inaccessible for attack on NAD^+. Therefore, transition-state formation requires an altered $G_{i\alpha1}$ conformation to expose and ionize Cys. The transition state has been docked into the crystal structure of pertussis toxin in a geometry required for transition state formation.

The biological action of the class of bacterial exotoxins which includes pertussis and cholera toxins is to ADP-ribosylate[1] several G-proteins including G_i, G_O, G_S, and transducin (*1, 2*). These GTP-binding proteins are trimers, consisting of α, *β*, and *γ*-subunits and are involved in the signal-transduction between membrane-bound receptors and the first enzyme in the related cascade, e.g., adenylate cyclase or phospholipases (*3, 4*). The mechanism by which G-proteins regulate signal transduction involves dissociation of the $\alpha\beta\gamma$ complex from the receptor following receptor activation, binding of a GTP-molecule to the α-subunit and dissociation of the trimer to form the α-subunit and a $\beta\gamma$-dimer. The dissociated state is the active state for the regulatory function. Reassociation of the trimer occurs after hydrolysis of GTP by the GTPase activity of the α-subunits, followed by rebinding to the membrane receptor.

Pertussis toxin from *Bordetella pertussis* ADP-ribosylates a cysteine side chain four amino acids from the C-terminus of the α-subunits of G_i, G_O, and G_T and prevents the binding of the G-protein trimer to its receptor (*5, 6*). Failure of the G-protein complex to interact at the membrane receptor site interrupts the regulation of cell functions by the related cascade (*7, 8*). Efficient ADP-ribosylation by pertussis toxin requires the complete $\alpha\beta\gamma$ trimer, and at least catalytic amounts of the $\beta\gamma$-subunits are necessary for significant catalysis in vitro (*9*). Isolated α-subunits are reported to be poor substrates for ADP-ribosylation by pertussis toxin. Pertussis toxin does not catalyze the ADP-ribosylation of low molecular weight thiols as model acceptors, as has been shown for cholera toxin with guanidinium compounds (*10, 11*). The peptide α_{i3}C20, which corresponds to the 20 C-terminal amino acids of $G_{i\alpha3}$, is a minimal substrate acceptor and has been used in kinetic and mechanistic studies (*12*−*14*). However, the peptide represents only a small portion of the biological acceptor, corresponding to 20 of the 354 amino acids of the α-subunit. Formation of the complex between pertussis toxin, NAD^+ and $G_{i\alpha1}$ is of interest in characterizing the ADP-ribosylation of a G-protein. The crystal structures of both $G_{i\alpha1}$ (*15*) and pertussis toxin (*16*) have been solved. The structures permit interpretation of the transition state chemistry in the context of known protein structures.

The ADP-ribosylation catalyzed by bacterial exotoxins is a major factor in the cytotoxicity of bacterial infections since loss of G-protein function often causes cell death. The development of transition-state analogues as inhibitors against the toxins has the potential to result in new agents for therapy against these infections. Transition-state structures can be deduced from the analysis of kinetic isotope effects of substrates specifically labeled around the reaction center, provided that chemical bond breaking occurs in a step which gives intrinsic or readily interpreted isotope effects (*17*). This method has been successful for several N-ribohydrolases (*18*−*21*), including cholera (*22*) and diphtheria (*23*) toxins, which hydrolyze NAD^+ into ADP-ribose and nicotinamide in the absence of acceptors. A family of powerful transition-state inhibitors has been synthesized for one nucleoside N-ribohydrolase on the basis of transition-state structural studies (*24*−*27*).

Transition-state studies on pertussis toxin have been performed for both NAD^+ hydrolysis and for ADP-ribosylation of the model acceptor α_{i3}C20 (*28, 29*). ADP-ribosylation of α_{i3}C20 was the most complex transition-state

† This work was supported by NIH research Grant AI34342.

* Author to whom correspondence should be addressed. Phone: (718) 430-2813. Fax: (718) 430-8565. E-mail: vern@aecom.yu.edu.

‡ Current address: Friedrich-Schiller-Universitaet Jena, Institut fuer Ultrastrukturforschung, Ziegelmuehlenweg 1; D-07743 Jena, Germany.

[1] Abbreviations: NAD^+, nicotinamide adenine dinucleotide, oxidized form; NMN, nicotinamide mononucleotide; ADP-ribose, adenosine diphosphoribose; KIE, kinetic isotope effect; DTT, dithiothreitol; TCA, trichloroacetic acid.

S0006-2960(97)02594-4 CCC: $15.00
Published on Web 02/13/1998

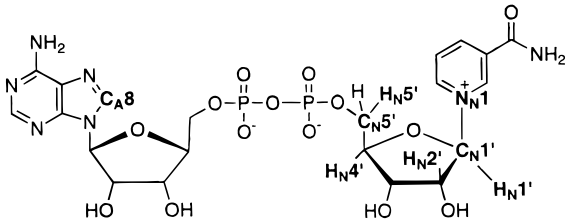

FIGURE 1: Structure of NAD^+ indicating positions in the molecule which were labeled with ^3H, ^{14}C, or ^{15}N, for kinetic isotope effect measurements.

structure solved by kinetic isotope effect methods. In the work reported here, the goal was to extend these studies to an even more complicated system, the ADP-ribosylation of the native $G_{i\alpha1}$ subunits expressed in the soluble form (*30*). Systematic isotope effect studies have not been reported on a system as complex as the ADP-ribosylation of $G_{i\alpha1}$ subunits. It is usually assumed that the enzymatic covalent modification of large substrates is limited by conformational changes which obscure kinetic isotope effects arising from the chemical step. The results reported here are remarkable in that nearly full expression of intrinsic isotope effects are observed in this complex system, permitting complete interpretation of the atomic details of transition-state structure. This study describes the steady-state kinetics, substrate commitment factor, kinetic isotope effects, and the transition-state structure for the ADP-ribosylation of recombinant α-subunits of the G-protein $G_{i\alpha1}$ catalyzed by pertussis toxin.

MATERIALS AND METHODS

Materials. Pertussis toxin A protomer was from List Biological Laboratories (Campbell, CA). The molecular weight of the A protomer as encoded by *Bordetella pertussis* is 26 220 (*31*). ^3H-, ^{14}C-, and ^{15}N-labeled NAD^+ samples (Figure 1) were prepared by enzymatic synthesis using published methods (*32*). [8_A-^{14}C]NAD^+ was prepared in a one-step procedure using nicotinamide mononucleotide instead of nicotinate mononucleotide. The *Escherichia coli* strain BL21(DE3) harboring the His-6 tagged gene of $G_{i\alpha1}$ was a generous gift from Dr. A. Gilman, Southwestern Medical Center, University of Texas. The molecular mass of expressed $G_{i\alpha1}$ is 41.5 kDa. Cells were grown in a double LB-medium as described by Lee et al. (*30*). The $G_{i\alpha1}$ subunits were purified on a Qiagen Ni-NTA-column (*30*), and concentrated to 80 mg/mL by ultrafiltration on Amicon YM-30 membranes or Centriprep 30 tubes. Protein concentration was determined with the Bio-Rad protein assay. G-protein β- and γ-subunits were purified from bovine brain by published methods (*9, 33*).

ADP-Ribosylation Assay. Reaction mixtures of 100 μL contained 0.2 μg of pertussis toxin and variable concentrations of $G_{i\alpha1}$ subunits in 100 mM Tris/HCl, pH 8.0, 20 mM DTT, and 1 mM EDTA. The mixture was incubated for 30 min to activate the toxin. The reaction was started by adding NAD^+ to 200 μM (or as indicated in the figures) and 25 000 cpm of [8_A-^{14}C]NAD^+, followed by incubation at 30 °C. Samples of 20 μL were taken at time = 0 and at appropriate time intervals, usually 20 min. The samples were added to 40 μL of a solution containing 1 mM unlabeled NAD^+ and 0.5% SDS and precipitated by adding of 60 μL 30% TCA solution. The precipitate was washed with 0.5 mL 5% TCA-solution followed by 0.5 mL diethyl ether and dissolved in 0.5 mL of 10% SDS in 200 mM Tris/HCl, pH 8.0. The samples were mixed with 9 mL of scintillation fluid and analyzed by scintillation-counting to quantitate the ADP-ribose coprecipitating with protein. Control samples indicated no ADP-ribosylation without pertussis toxin and that >99.5% of unreacted NAD^+ was removed by the washing procedures. Concentrations of unreacted NAD^+ were determined from the combined TCA supernatants. Product formation was determined from the radioactivity of the dissolved precipitate.

Commitment to Catalysis. Reaction mixtures of 10 μL containing 20 μM activated pertussis toxin and 200 μM NAD^+ including 70 000 cpm [8_A-^{14}C]NAD^+ were incubated for 15 s at the indicated temperatures. A solution containing 100 μL of 10 mM unlabeled NAD^+ and variable amounts of $G_{i\alpha1}$ subunits was added, and the mixture was incubated to allow approximately 10 catalytic turnovers. In control experiments, samples of 110 μL containing the identical amounts of pertussis toxin, labeled and unlabeled NAD^+, and G-protein were incubated for the same time. The reactions were stopped by addition of 100 μL 30% TCA solution and treated as described above.

Solvent Kinetic Isotope Effects. Reaction mixtures for the pertussis toxin initial rate assay were prepared with variable substrate concentrations and D_2O content. Samples of $G_{i\alpha1}$ were concentrated in Amicon Microcon-30 tubes and dissolved in buffer with variable H_2O/D_2O. This was repeated three times. All other reagents were lyophilized and dissolved in variable ratios of H_2O/D_2O. Initial reaction rates were determined by the ADP-ribosylation assay as described above. NAD^+ was held constant at 200 μM and the concentrations of the $G_{i\alpha1}$ subunits were varied from 100 to 900 μM.

Kinetic Isotope Effects. NAD^+ samples containing approximately 100 000 cpm of each of the isotopes in the sensitive and in the remote positions were adjusted with unlabeled NAD^+ to give a final concentration of 100 μM in the sample. The mixtures were purified on Nucleosil RP18 HPLC columns (7.9 × 300 mm) with an eluent of 50 mM ammonium acetate, pH 5.0, and lyophilized. Identical reaction mixtures were converted to products to the extent of 20−40% of total NAD^+ for one sample and to 100% conversion of NAD^+ with the companion sample. Reaction mixtures of 400 μL contained 2 μg/mL of pertussis toxin A-protomer for the 20−40% reaction and 3.7 μg/mL for the 100% reaction. Both contained 0.6 mM of purified $G_{i\alpha1}$ subunits in 100 mM Tris/HCl, pH 8.0. The assay mixtures were incubated for 30 min to activate the toxin. The reaction was started by adding NAD^+ to the sample. The reaction for 20−40% product formation was incubated for 45 min at 30 °C, and that for 100% conversion for 3 h at 4 °C. The reaction at 4 °C was necessary for quantitative conversion of NAD^+ to the ADP-ribosylated G-protein during the extended incubation to ensure complete conversion to products. Aliquots of 100 μL were added to 200 μL of stop solution containing 1 mM unlabeled NAD^+ and 0.5% SDS and precipitated by adding 300 μL 30% TCA. The samples were treated as described for the ADP-ribosylation assay. The $^3H/^{14}C$ ratios of the partial reaction (approximately 30% conversion to product) and the complete reaction were

determined by scintillation counting. A standard ^{14}C-sample was prepared by precipitating 2 mg of $G_{i\alpha1}$ subunits in a reaction mixture treated in the same way as those samples used to determine the kinetic isotope effects. In these controls, the radioactivity standard was provided by ^{14}C-glucose. Addition of the protein was necessary to adjust for small quenching effects in the scintillation vial caused by the protein. The samples of each experiment were counted for at least 10 cycles of 10 min/sample and the resulting KIE's were calculated (*34*).

Transition-State Model. The transition-state structure was determined using the structure interpolation approach to bond order vibrational analysis (*35*). Trial transition-state structures are generated systematically by interpolation between reference structures for the reactant and the fully dissociated (ribo-oxocarbenium ion plus nicotinamide) structure. The reactant and trial transition state cutoff structures were defined, along with force constants for bond stretches, bond angle bends, and bond torsions. The program BEBOVIB (*36*) calculates the KIE at each isotopically labeled position using the isotopic partition function of Bigeleisen and Wolfsberg (*37*). The point in reaction coordinate space where the calculated KIEs most closely matched the measured ones located the transition-state structure (see ref *35*).

Docking the Transition-State Structure and $G_{i\alpha1}$ with Pertussis Toxin. The transition-state structure used for docking included all the atoms of NMN^+ and the sulfur nucleophile. It was docked into the catalytic site of pertussis toxin as described below. Pertussis toxin is not catalytically active until the Cys41−Cys201 disulfide bond is reduced (*38*). In the X-ray crystallographic model of pertussis toxin holoenzyme, this disulfide is intact (*16*) and residues 190−206 occupy the proposed active-site cleft. Deletion of the 55 C-terminal residues of the catalytic domain decreases k_{cat}/K_M for the ADP-ribosylation reaction, but not for NAD^+ hydrolysis, implying that the C-terminal peptide is important for binding of $G_{i\alpha1}$, but not for the chemical steps (*39*). To create an open active-site cleft, the C-terminus residues 189−235 were deleted, and the remaining structure was superimposed on the X-ray crystallographic structure of diphtheria toxin with substrate NAD^+ bound in the active site (*40*). The Cβ atoms of the catalytic Glu129 in pertussis and Glu148 in diphtheria and the backbone atoms of homologous residues (*41*) in the β-strands were superimposed. Following this procedure, the bound NAD^+ from the diphtheria toxin crystal structure fit with good complementarity and without steric clashes into the active site cleft of pertussis toxin.

The transition-state structure was docked in the active site by adjusting its position to optimize interactions between the oxocarbenium ion and Glu129 and to place the nicotinamide ring in the presumed binding pocket. The orientations of the ribosyl and nicotinamide rings relative to each other were allowed to vary. With the weak N-ribosidic bond at the transition state, changes in the angle between the nicotinamide ring and the ribosyl moiety would have a negligible effect on the energetics of the transition-state structure. Once the position of the transition-state structure was fixed, torsional angles about C4′−C5′, C5′−O5′, and O5′−P were altered to allow optimum interactions between the ADP-portion of NAD^+ and diphtheria toxin. The ADP-moiety was moved less than 1 Å to optimize interactions in the transition-state model for pertussis toxin.

Structural changes to the pertussis toxin structure during docking were minimal. The side chain of Glu129 was rotated to make it more similar to the position of Glu148 in diphtheria toxin and to optimize its interactions with the transition-state structure. The side chains of residues Tyr126 and Leu123 were rotated to improve interactions with the $G_{i\alpha1}$ (see below). The side chain of Gln127 was rotated to improve the visibility of the nicotinamide bound in the active site, but there was no structural requirement for this movement.

The 10 C-terminal amino acids of $G_{i\alpha1}$ were modeled as a fully extended polypeptide. The nucleophilic Cys351 residue was placed in the correct orientation relative to the NAD^+ transition state, and backbone or side chain orientations were adjusted to form favorable interactions with pertussis toxin and/or the NAD^+ transition state.

RESULTS

Kinetic Studies. Isolated $G_{i\alpha1}$ subunits and related α-subunits are reported to be weak substrates for ADP-ribosylation by pertussis toxin, and require catalytic amounts of the $\beta\gamma$-subunit complex (*9*). Experiments were designed to characterize the effect of $\beta\gamma$-subunits on the ADP-ribosylation of $G_{i\alpha1}$ subunits. In the absence of $\beta\gamma$-subunits and at concentrations of recombinant α-subunits above 25 μM, slow but significant ADP-ribosylation of $G_{i\alpha1}$ subunits was observed at temperatures between 4 and 37 °C (Figure 2A). Addition of substoichiometric amounts of $\beta\gamma$-subunits from bovine brain to the $G_{i\alpha1}$ subunits resulted in an increase of activity as expected at $G_{i\alpha1}$ subunit concentrations below 100 μM (Figure 2B). Increasing the α-subunit to a concentration above 100 μM resulted in a $\beta\gamma$-independent ADP-ribosylation of $G_{i\alpha1}$ subunits. The use of α-subunits at concentrations of 500 μM gave rapid ADP-ribosylation which permitted formation of sufficient product for kinetic isotope effect studies. Quantitative conversion of labeled NAD^+ into ADP-ribosylated $G_{i\alpha1}$ subunits is required as a control for the kinetic isotope effect procedure and was readily accomplished at 4 °C.

Initial rate studies with pertusis toxin indicated $k_{cat} = 40 \pm 9$ min^{-1} and $K_m = 800 \pm 300$ μM for ADP-ribosylation of $G_{i\alpha1}$ subunits at pH 8.0 in 100 mM Tris/HCl at 30 °C. The K_m for NAD^+ was 23 ± 3 μM under these conditions. The k_{cat} is similar to that reported for the ADP-ribosylation of the $\alpha\beta\gamma$-trimer of G_T by pertussis toxin (*39*). The large difference in the K_m values for $G_{i\alpha1}$ in the presence and absence of $\beta\gamma$ indicates the low affinity of the monomeric α-subunit relative to the trimeric complex (Table 1). The catalytic behavior of the $\beta\gamma$ subunits in promoting ADP-ribosylation establishes that the addition to $G_{i\alpha1}$ and release of $\beta\gamma$ following ADP-ribosylation of $G_{i\alpha1}$ in the trimeric complex are both rapid relative to catalysis. The K_m for NAD^+ with pertussis toxin is similar for ADP-ribosylation of the trimer (*39*), ADP-ribosylation of $G_{i\alpha1,}$ ADP-ribosylation of the peptide α_{i3}C20, and for NAD^+ hydrolysis (*29*). The results suggest that NAD^+ interaction with pertussis toxin is independent of the G-protein substrate structure. Kinetic parameters for the reactions catalyzed by pertussis toxin are summarized in Table 1.

Kinetic parameters for ADP-ribosylation of $G_{i\alpha1}$ protein by pertussis toxin were determined as a function of pH in

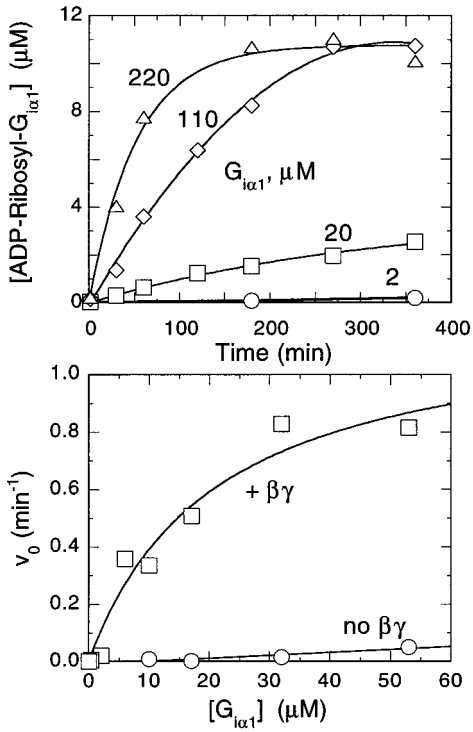

FIGURE 2: (Top) ADP-ribosylation of recombinant $G_{i\alpha1}$ subunits catalyzed by pertussis toxin in the absence of $\beta\gamma$-subunits and as a function of $G_{i\alpha1}$ concentration. Samples contained 2.5 μg/mL (0.1 μM) pertussis toxin, the indicated concentration of $G_{i\alpha1}$ and 11 μM NAD^+ including [8_A-^{14}C]NAD^+ in 100 mM Tris/HCl, pH 8.0, 20 mM DTT, and 1 mM EDTA. The assays were performed at 4 °C. In the presence of both 110 and 220 μM $G_{i\alpha1}$, the ADP-ribosylation is complete at 300 min. (Bottom) ADP-ribosylation of $G_{i\alpha1}$ subunits by pertussis toxin in the absence (open circles) and presence (open squares) of catalytic amounts of $\beta\gamma$-subunits. Samples contained 2 μg/mL (0.08 μM) pertussis toxin, variable concentrations of $G_{i\alpha1}$ subunits, and 30 μM NAD^+ including [8_A-^{14}C]NAD^+ in 100 mM Tris/HCl, pH 8.0, 20 mM DTT, and 1 mM EDTA. Assays which included $\beta\gamma$-subunits (open squares) contained approximately 0.2 μg/mL $\beta\gamma$-subunits isolated from bovine brain.

the range 6.0−9.0. The K_m for NAD^+ was nearly constant, near 20 μM. A decrease in k_{cat} values was found at pH >8.0. Both k_{cat} and k_{cat}/K_m were maximal between pH 7.0 and 8.0. Kinetic parameters were also determined in the presence of the GTP analogue GTPγS, or with GDP. Crystal structures of $G_{i\alpha1}$ subunits in the presence of these compounds have demonstrated some differences in the C-terminal region where ADP-ribosylation occurs (*15*, *42*). An increase of the K_m value for $G_{i\alpha1}$ subunits from 800 to 1600 μM was observed in the presence of GTPγS. The K_m found in the presence of GDP was 900 μM, which is not a significant increase. The k_{cat} values were found to be independent of the presence of guanine nucleotides.

Commitment to Catalysis. The probability that NAD^+ bound in the NAD^+·toxin·$G_{i\alpha1}$ Michaelis complex will be converted to product relative to release as unchanged NAD^+ is defined as the commitment to catalysis (*19*, *43*). Under conditions where 7000 cpm of NAD^+ were bound to pertussis toxin in the binary complex, dilution into excess unlabeled NAD^+ and variable $G_{i\alpha1}$ followed by several catalytic turnovers resulted in <150 cpm converted to ADP-ribosylated $G_{i\alpha1}$ at saturating $G_{i\alpha1}$ concentration. Similar results were obtained in isotope trapping experiments at both 4 and 30 °C. The small amount of the ADP-ribosyl product formed in substrate trapping experiments established a commitment factor below 0.02. Substrate committed to catalysis decreases the experimentally observed isotope effects. The small commitment factor for NAD^+ is well below that which could have a significant influence on the measured kinetic isotope effects.

Solvent Isotope Effects. An inverse solvent deuterium isotope effect of 0.65 ± 0.07 for k_{cat} was found for the ADP-ribosylation of the $G_{i\alpha1}$ subunit. The solvent isotope effect for k_{cat}/K_m was smaller, but at 0.9 ± 0.1 may also be slightly inverse. An increase of the K_m value for the α-subunit from 800 to 1200 μM was measured in the presence of D_2O. The binding of the large G-protein to the toxin provides numerous contacts between the proteins which could result in normal isotope effects of binding. The K_m value in 90% D_2O is about 30% higher than in H_2O, resulting in a small, inverse k_{cat}/K_m solvent isotope effect. Pre-transition-state deprotonation of the nucleophilic thiol group is consistent with the inverse solvent isotope effect on k_{cat}. Inverse solvent isotope effects are usually caused by preequilibrium steps in which the active species, in this case the thiolate anion, is favored in the presence of D_2O (*44*).

Kinetic Isotope Effects. Kinetic isotope effects were measured as a function of temperature and pH. KIEs measured at 4 °C showed smaller values than expected from the analogous reaction of the ADP-ribosylation of peptide α_{i3}C20 at this temperature (*29*). The kinetic isotope effect from [$1'_N$-^{3}H]NAD^+ was used to examine the influence of temperature and pH on the experimental expression of isotope effects. The KIE at this position is the largest of those measured and is therefore the most sensitive to changes by variation of the reaction conditions. Kinetic isotope effects were determined at temperatures between 4 and 37 °C, and indicate an increase of the KIE from 1.12 to 1.19 between 4 and 20 °C (Figure 3A). Between 20 and 37 °C, only a slight increase to 1.20 was observed. This behavior cannot be explained by an increased commitment to catalysis at low temperature, since this is known to be negligible at both 4 and 30 °C (see above).

The [$1'_N$-^{3}H] KIE was also measured between pH 6.0 and 9.0, (Figure 3B). The observed KIE is 1.16 below pH 7.0 and increases to approximately 1.20 above pH 7.5. The dependence of KIE on pH and temperature for ADP-ribosylation of $G_{i\alpha1}$ subunits is in contrast to the behavior of pertussis toxin for NAD^+ hydrolysis and the ADP-ribosylation of the peptide α_{i3}C20. In these reactions the [$1'_N$-^{3}H] was constant over the same pH range, demonstrating that the effect is specific for $G_{i\alpha1}$ subunits.

The family of KIEs used to determine the transition-state structure was measured at 30 °C and pH 8.0, where the maximum $1'_N$-^{3}H isotope effect was observed. The reference experiments in which 100% of the labeled NAD^+ was converted to ADP-ribose-$G_{i\alpha1}$ were performed at 4 °C. This prevented significant NAD^+ hydrolysis by pertussis toxin which occurs in parallel to ADP-ribosylation at higher temperatures (*14*). At 30 °C, the rate of $G_{i\alpha1}$ peptide ADP-ribosylation is >50-fold greater than the rate of NAD^+ hydrolysis, and causes a negligible effect on the experimentally measured kinetic isotope effects. The catalytic rate for ADP-ribosylation is >100-fold faster than the rate of NAD^+ hydrolysis reaction at 4 °C and at high concentrations of $G_{i\alpha1}$.

Table 1: Kinetic Constants for Reactions Catalyzed by Pertussis Toxin

reaction	K_m NAD$^+$ (μM)	K_m acceptor (μM)	k_{cat} (min^{-1})	k_{cat}/K_m NAD$^+$ (M^{-1} s^{-1})	k_{cat}/K_m acceptor (M^{-1} s^{-1})
hydrolysis[a]	24 ± 5		0.4 ± 0.1	2.8×10^2	
peptide α_{i3}C20[b]	27 ± 9	69 ± 16	3.0 ± 0.3	1.9×10^3	7.2×10^2
$G_{i\alpha1}$ monomer[c]	23 ± 3	800 ± 300	40 ± 9	2.9×10^4	8.3×10^2
G_T trimer[d]	20 ± 2	0.3 ± 0.04	10 ± 0.4	8.3×10^3	5.6×10^5

[a] Conditions: 50 mM phosphate and 20 mM DTT, pH 7.5, 37 °C. [b] Conditions: 50 mM phosphate and 20 mM DTT, pH 7.5, 4 °C. [c] Conditions: 50 mM Tris/HCl and 20 mM DTT, pH 7.5, 30 °C. [d] Data from Cortina et al. (1991).

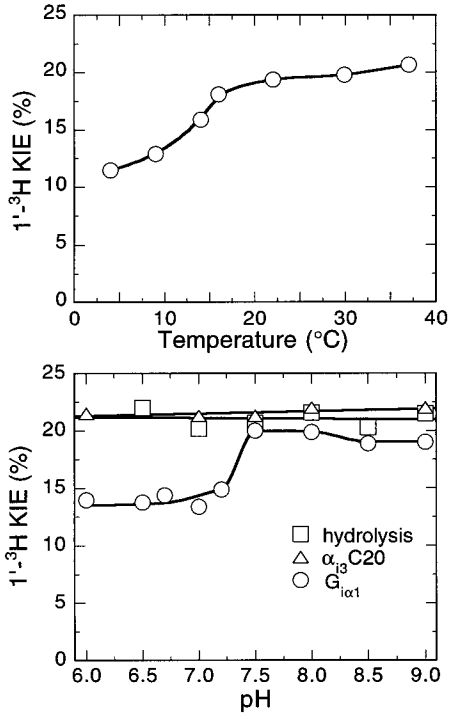

FIGURE 3: Kinetic isotope effects for ADP-ribosylation of $G_{i\alpha1}$ subunits by pertussis toxin as function of temperature (top) and pH (bottom). For comparison, the corresponding [$1'_N$-^{3}H]NAD$^+$ KIEs from NAD$^+$ hydrolysis (*28*) and ADP-ribosylation of the synthetic peptide α_{i3}C20 catalyzed by pertussis toxin (*29*) are included for the pH dependence. The ordinate scales are percent KIE where (KIE-1.00) × 100 = % KIE. The expected temperature-dependence of kinetic isotope effects in this range is given by $KIE_{310K} = \exp[(277/310)\ln(KIE_{277K})]$, or a change from 1.199 to 1.176, much smaller than observed.

The primary [$1'_N$-^{14}C] KIE = 1.049 ± 0.003 for the transfer reaction was larger than that for NAD$^+$ hydrolysis catalyzed by pertussis toxin, 1.021 ± 0.001, while the [1_N-^{15}N] KIE = 1.022 ± 0.004 was similar to that for the hydrolytic reaction, 1.021 ± 0.004. This difference indicates that the transition state for the ADP-ribosylation of $G_{i\alpha1}$ exhibits greater bond order to the nucleophile and less oxocarbenium ion character at the transition state than does the hydrolytic reaction.

The experimental double primary KIE = 1.069 ± 0.003 was within experimental error of the product of the single primary KIEs (1.072 ± 0.007). This is a necessary consequence (though not diagnostic) of a mechanism where both isotope effects arise from a single step. The equality of those values also demonstrates the accuracy of the KIE measurements.

The α-secondary [$1'_N$-^{3}H] KIE was 1.199 ± 0.009, and the β-secondary [$2'_N$-^{3}H] KIE was 1.105 ± 0.004. Both values indicate an oxocarbenium-ion-like character of the ribose ring at the transition state. This structure allows increased freedom for the out-of-plane bending mode of the C1′−H1′ bond and hyperconjugation of the C2′−H2′ bond with the developing p-orbital of C1′.

The isotope effects of 0.991 ± 0.002 and 1.020 ± 0.004 for the remote [$4'_N$-^{3}H] and [$5'_N$-^{3}H] positions are typical of N-ribohydrolase reactions. Because the isotope effects at these positions are small for chemical solvolysis (Table 2), these isotope effects must arise from interactions of the enzyme with NAD$^+$ remote from the C1′-N1 bond (*22*, *35*).

Transition-State Model. The transition-state structure was determined using the structure interpolation approach to bond energy/bond order vibrational analysis (*35*). The transition state was defined by the point in reaction coordinate space where the KIEs for trial transition-state structures most closely matched the experimental KIEs (Figure 4). This occurred when the residual bond order to the leaving group nicotinamide, n_{LG}, was 0.11 (bond length = 2.12 Å), and the bond order to the approaching nucleophile, n_{Nu}, was 0.085 (2.55 Å).

The predicted KIEs for the $1'_N$-^{14}C, 1_N-^{15}N and $2'_N$-^{3}H labels were within ± 0.001 of the experimental KIEs (Table 2). The predicted $1'_N$-^{3}H KIE = 1.055 differed from the measured KIE of 1.199 ± 0.009. On the basis of previous experimental evidence (*45*−*49*) and quantum mechanical calculations (*50*−*52*), the $1'_N$-^{3}H KIE (1.199 ± 0.009) for the more concerted pertussus toxin reaction would have been expected to be lower than for the hydrolytic reactions of NAD$^+$, which proceeds through more dissociative transition states (*22*, *23*, *28*, *35*; e.g. $1'_N$-^{3}H KIE = 1.207 ± 0.010 for NAD$^+$ hydrolysis by pertussis toxin). The cause of this discrepancy is not known; however, it does not change the overall transition-state structure. The predicted $1'_N$-^{3}H KIE could be increased to match the experimental KIE by decreasing the bond bending (N1−C1′−H1′ and S−C1′−H1′) and the H1′ out-of-plane bending force constants. This changed the other predicted KIEs by less than 0.002. Because it is possible to match the experimental KIE through different combinations of altered force constants in the transition state, and because the reason for requiring the decreased bending force constants is not yet clear, we have simply reported the originally predicted $1'_N$-^{3}H KIE =1.055. Continuing studies to improve the prediction of $1'_N$-^{3}H KIE's by ab initio methods are underway.

DISCUSSION

This study describes kinetic isotope effect studies on the ADP-ribosylation of $G_{i\alpha1}$ by pertussis toxin, leading to a full transition-state structure. The structure is docked into the crystal structure of the toxin to provide a working model

Table 2: Kinetic Isotope Effects for the ADP-Ribosylation of the $G_{i\alpha1}$ Subunits by Pertussis Toxin

substrates	sensitive isotopic label	toxin KIE	solvolysis KIE[c]
[$1'_N$-^{14}C]- and [$4'_N$-^{3}H]NAD^+	^{14}C, primary[a]	1.049 ± 0.003 (3)[b]	1.016 ±0.002
[1_N-^{15}N]- and [$4'_N$-^{3}H]NAD^+	^{15}N, primary[a]	1.023 ± 0.004 (4)	1.020 ± 0.007
[1_N-^{15}N, $1'_N$-^{14}C]- and [$4'_N$-^{3}H]NAD^+	^{15}N and ^{14}C double-primary[a]	1.069 ± 0.003 (2)	1.034 ± 0.002
[$1'_N$-^{3}H]- and [$5'_N$-^{14}C]NAD^+	^{3}H, α-secondary	1.199 ± 0.009 (4)	1.194 ± 0.005
[$2'_N$-^{3}H]- and [$5'_N$-^{14}C]NAD^+	^{3}H, β-secondary	1.105 ± 0.004 (4)	1.114 ± 0.004
[$4'_N$-^{3}H]- and [$5'_N$-^{14}C]NAD^+	^{3}H, γ-secondary	0.991 ± 0.002 (4)	0.997 ± 0.001
[$5'_N$-^{3}H]- and [$5'_N$-^{14}C]NAD^+	^{3}H, δ-secondary	1.020 ± 0.004 (3)	1.000 ± 0.003

[a] Observed isotope effects were corrected by the formula (obs. KIE × [4′-^{3}H]KIE). [b] The numbers in parentheses is the number of independent experiments, each of which analyzed quadruplicate samples of KIE reaction mixtures. [c] Hydrolysis of NAD^+ was at 100 °C in 50 mM sodium acetate buffer pH 4.0. The data are taken from ref 35. The data are not corrected for the temperature effect on kinetic isotope effects.

Table 3: Bond Order and Bond Length for NAD^+ Reactant and Transition-State Structures of the ADP-Ribosylation of the $G_{I\alpha1}$ Subunits by Pertussis Toxin A Protomer

	reactant state		transition state	
bond[a]	bond order	Å[b]	bond order	Å[b]
C1′−N1	0.77	1.55	0.11	2.13
C1′−O4′	0.95	1.42	1.39	1.31
C1′−C2′	0.87	1.57	1.03	1.52
C1′−H1′	1.03	1.08	1.06	1.07
C2′−H2′	1.008	1.088	0.986	1.094
C1′−nucl.			0.085	2.55

[a] All bonds refer to those in the NMN^+ portion of the NAD^+ molecule (Figure 1). [b] Bond lengths for the reactant NAD^+ are taken from X-ray crystal structures and are summarized in ref 35. Bond lengths and bond orders in the transition state are less certain than in the reactant, and depend on the accuracy of the KIE measurements and the computational algorithms which match the transition state bonds to the KIE. A comprehensive discussion of these factors is provided by Huskey (*56*). Uncertainty limits of 0.1, 0.03, 0.01, 0.002, 0.001, and 0.1 Å can be estimated for the C1′−N1, C1′−04′, C1′−C2′, C1′−H1′, C2′−H2′, and C1′−nucleophile bonds based on the sensitivity of the calculated KIE to bond order and the errors of the KIE measurements (Table 2).

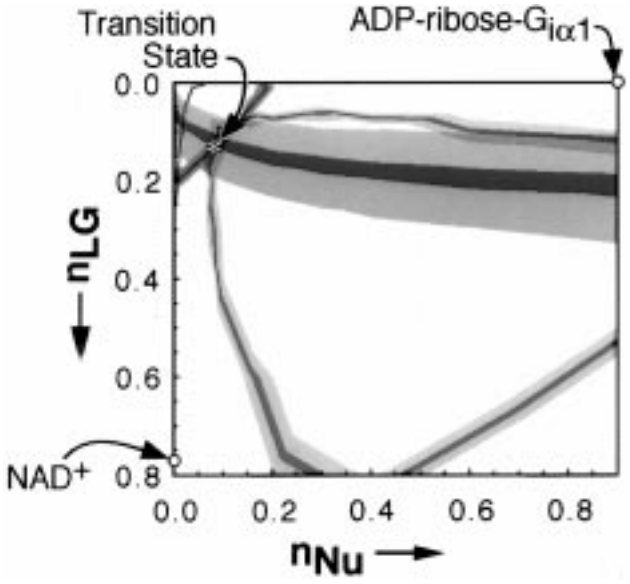

FIGURE 4: Match of predicted versus experimental KIEs. For each isotopic label, the colored area represents the match of the predicted with the experimental KIEs as a function of the bond order to the leaving group (n_{LG}) and the bond order to the attacking nucleophile (n_{Nu}) in reaction coordinate space. The light shading represents the 95% confidence interval of each measured KIE, with dark shading representing the measured KIE (approximately ± 0.001): blue = 1_N–15N, red = $1'_N$-14C, gray = $1'_N$-3H, green = $2'_N$-3H. The predicted transition-state structure is indicated by an asterisk (∗). Reactant NAD^+ is in the lower left corner of reaction coordinate space and product ADP-ribosylated α-subunit is in the upper right, labeled "ADP-ribose-$G_{i\alpha1}$".

for the mechanism of G-protein modification. The discussion addresses three unique contributions from this work: (*1*) the ability of pertussis toxin to ADP-ribosylate isolated, recombinant α-subunits in the absence of $\beta\gamma$-subunits, (*2*) the measurement of intrinsic kinetic isotope effects using high molecular weight complexes in protein covalent modifications, and (*3*) the mechanism and transition-state structure for the ADP-ribosylation of $G_{i\alpha1}$ protein by pertussis toxin.

Kinetic Properties for the ADP-Ribosylation of $G_{i\alpha1}$ by Pertussis Toxin. Isolated α-subunits have been reported to be poor substrates for the ADP-ribosylation catalyzed by pertussis toxin (*9*). Previous studies were performed in the physiological range of nanomolar to micromolar α-subunit concentrations. The reaction with $G_{i\alpha1}$ follows Michaelis−Menten kinetics with K_m = 800 ± 300 μM, about 2000-fold greater than that of 0.3 μM for the $\alpha\beta\gamma$ trimer (*39*). In contrast, k_{cat} is nearly the same, thus the chemical step is unaffected by the $\beta\gamma$-subunits. The synthetic peptide α_{i3}-C20, has been used as an ADP-ribose acceptor and exhibits a K_m value an order of magnitude smaller than the α-subunit (*29*). Contacts between the α-subunit and pertussis toxin are therefore likely to occur primarily in the C-terminal amino acids. The $\beta\gamma$-subunits can act by promoting favorable contacts of the α-subunit with pertussis toxin or by relieving unfavorable contacts between $G_{i\alpha1}$ and the toxin. Additional contacts which increase the affinity between pertussis toxin and the complete trimer are therefore provided by the β- and/or γ-subunits.

The presence of GDP and GTPγS can stabilize different conformations of the $G_{i\alpha1}$ subunits, as shown by X-ray crystallography. However guanine nucleotides have only minor effects on the ADP-ribosylation of $G_{i\alpha1}$ by the toxin in the absence of $\beta\gamma$-subunits. Addition of GTPγS, which favors $\alpha\beta\gamma$ dissociation to monomeric α-subunits, resulted only in a minor decrease in catalytic efficiency as indicated by the k_{cat}/K_m value. Binding of GDP favors formation of the $\alpha\beta\gamma$ trimer in the regulatory cycle of G-proteins, but also yielded only an insignificant change in activity. The reported increased activity of ADP-ribosylation in the presence of GDP with catalytic amounts of $\beta\gamma$-subunits (*9*) therefore results from the formation and stabilization of the $\alpha\beta\gamma$ complex as a result of GDP-binding. The increased affinity of the $\alpha\beta\gamma$ complex for pertussis toxin relative to $G_{i\alpha1}$ results in the observed activity increase.

Transition-state analysis of the ADP-ribosylation reaction with pertussis toxin $G_{i\alpha1}$ requires the formation of a ternary

enzyme·NAD^+·acceptor protein complex, since the inversion of configuration at C1′ of NAD^+ establishes a displacement mechanism and eliminates the possibility of an enzyme-ADP-ribose covalent intermediate (*14*). The $G_{i\alpha1}$ subunit, has a molecular mass of 42 kDa and that of pertussis toxin A-chain is 26 kDa. Protein−protein interactions can be slow, and thus obscure chemical steps in protein covalent modifications. It was essential to quantitate relative rates of protein binding and release in comparison to catalysis. Isotope trapping experiments showed no significant forward commitment at 30 °C. The experimental isotope effects are in agreement with those for the ADP-ribosylation of the α_{i3}-C20 by pertussis toxin, a simpler reaction which has no catalytic commitment, and exhibits intrinsic kinetic isotope effects (*29*). These experiments demonstrate that the kinetic isotope effects for the ADP ribosylation of $G_{i\alpha1}$ subunit at pH 8.0 and 30 °C are intrinsic. Intrinsic isotope effects can be used to interpret transition-state structure. This is the first indication that transition-state structures can be determined for the covalent modifications of regulatory proteins.

Reaction Energetics for ADP Ribosylation of $G_{i\alpha1}$ by Pertussis Toxin. The experimental $1'_N$-^{3}H KIE for $G_{i\alpha1}$-ADP ribosylation by pertussis toxin was both temperature and pH dependent. KIEs of 1.20 were observed at temperatures >20 °C and pH ≥7.5 (Figure 3B), descreasing to below 1.15 with decreasing temperature or pH. The temperature dependence was not due to forward commitment to catalysis since this was negligible at both 4 and 30 °C (see Results). This behavior of the $1'_N$-^{3}H KIE is consistent with a step in the reaction after the chemical step becoming kinetically significant. For example, a protein conformational change required for product release could become slow enough at low pH and low temperature to allow the enzyme-bound products, $G_{i\alpha1}$-ADP-ribose and nicotinamide, to undergo the reverse reaction to reform substrates $G_{i\alpha1}$ and NAD^+. This situation would cause a reverse commitment to catalysis, leading to decreased experimental KIEs, and is illustrated in Figure 5. The effects of commitments to catalysis are predicted by the expression of Northrup (*17*):

$$^3V/K = \frac{^3k + C_f + C_r\,^3K_{eq}}{1 + C_f + C_r} \quad (1)$$

where $^3V/K$ is the measured kinetic isotope effect from [$1'_N$-^{3}H]NAD^+, ^3k is the intrinsic isotope effect on the isotopically sensitive step, C_r and C_f are reverse and forward commitments, respectively, and $^3K_{eq}$ is the equilibrium isotope effect. There is no significant forward commitment with pertussis toxin. The C1′ of both NAD^+ and $G_{i\alpha1}$-ADP-ribose are sp^3-hybridized, therefore, the equilibrium isotope effect is near unity. This simplifies the expression to

$$^3V/K = \frac{^3k + C_r}{1 + C_r} \quad (2)$$

When the energetic barrier heights are equal for the catalytic step and the reverse commitment (C_r) is unity, half of the intrinsic isotope effect will be lost. A reaction energetics diagram demonstrates this effect (Figure 5). If the decreased isotope effects are due to reverse commitment, limits can be imposed from the pH and temperature dependence and

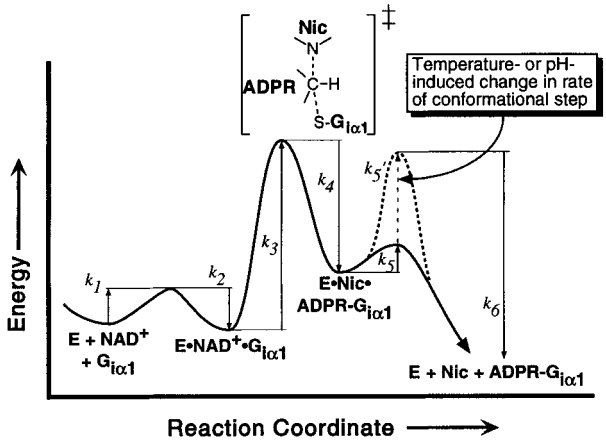

FIGURE 5: Reaction coordinate diagram for ADP-ribosylation of $G_{i\alpha1}$ subunits by pertussis toxin. The first two steps of NAD^+ and $G_{i\alpha1}$ subunit binding and release (k_1 and k_2) are combined into a single low-energy step, established by lack of NAD^+ commitment. The irreversible step is bond breaking and making (k_3 and k_4) based on the intrinsic kinetic isotope effects at pH 8.0 and 30 °C. The decrease in kinetic isotope effect at unfavorable temperatures and pH values is ascribed to reverse commitment (slow product release) since forward commitment does not occur. Based on the weak binding of products to pertussis toxin, it is proposed that k_5 is a slow protein conformational change which permits release of products.

eq 2. The decreased kinetic isotope effect at 4 °C and at values below pH 7 indicates that enzyme-bound $G_{i\alpha1}$-ADP-ribose and nicotinamide have a $^2/_3$ probability of release as products and a $^1/_3$ probability of reequilibrating with substrate. Slow product release can be caused either by tight binding of product or a protein conformational change associated with product release. The temperature and pH dependence of the 1′-^{3}H isotope effect establishes that one of these factors causes reverse commitment at temperatures <20 °C and pH <7.5. Since the product ADP-ribosyl-α_{i3}-C20 binds poorly, a protein conformational change is implicated (*14*).

The Transition-State Structure. The ADP-ribosylation of $G_{i\alpha1}$ by pertussis toxin proceeds with inversion of configuration, indicating a direct nucleophilic displacement of nicotinamide by Cys351. However, the approach of the nucleophile (bond order = 0.085, 2.5 Å) lags behind the loss of the leaving group (bond order 0.11, 2.1 Å), resulting in a transition state with oxocarbenium ion character due to accumulation of positive charge on the ribosyl ring of NAD^+ (Figure 6). This transition-state structure is more synchronous than for hydrolysis of NAD^+ by pertussis toxin. Using comparable analyses, weak bonds to nicotinamide (0.05) and to the attacking water nucleophile (0.001) are found for the hydrolysis reaction. The energy associated with the binding of $G_{i\alpha1}$ to the pertussis toxin·NAD^+ binary complex causes a 100-fold increase in k_{cat}/K_m and a change in transition-state structure. The biggest change is the 100-fold increase in the bond order to the attacking Cys351 for the ADP-ribosylation versus hydrolysis, as compared with a 2-fold increase in the bond order to nicotinamide. Presumably, the increase in rate and the change in transition-state structure is the result of having the highly nucleophilic thiolate anion of Cys351 from $G_{i\alpha1}$ poised for nucleophilic attack on NAD^+ as the C1′−N1 bond lengthens.

Docked Model of the Binary Pertussis Toxin·NAD^+ Transition-State Complex. Although the transfer reaction is

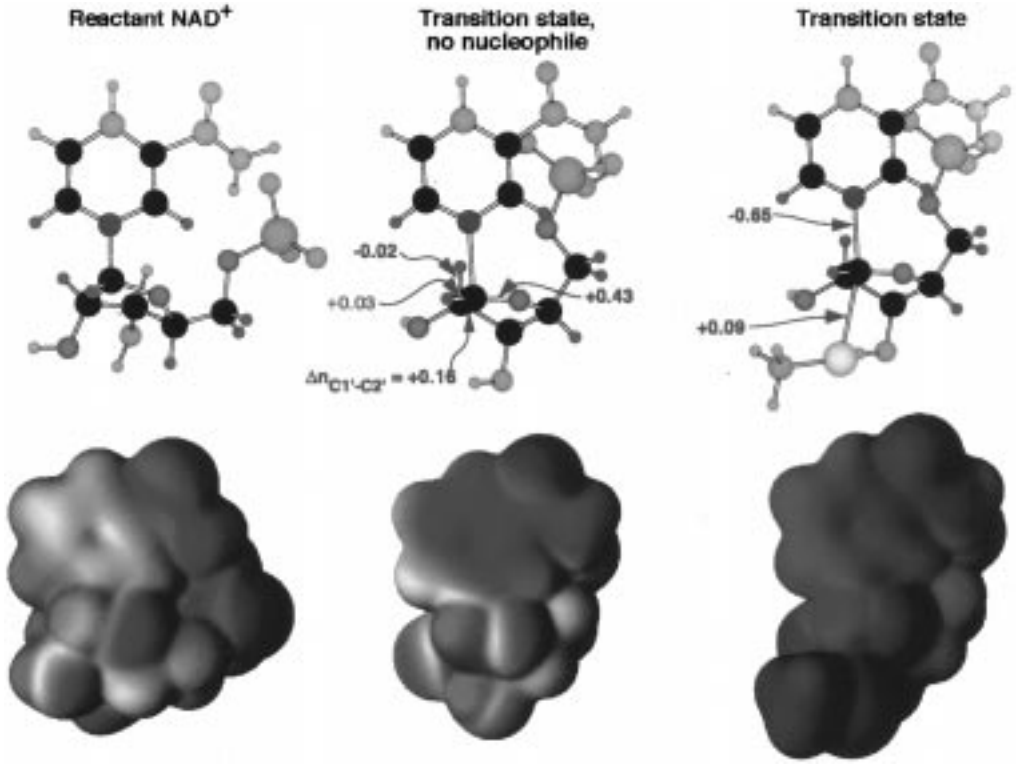

FIGURE 6: Structures of reactant NAD^+ and the transition state without and with a methyl thiolate nucleophile. The upper row is three ball-and-stick figures with atoms included in the BEBOVIB calculations (cutoff models) colored by element; all others are colored gray. Changes in bond order between the reactant and the transition states are indicated. A single covalent bond has bond order = 1.00. All atoms within two bonds of the isotopically labeled positions were included in KIE calculations, yielding proper cutoff models (*57*). The bottom row illustrates three electrostatic potential surfaces projected onto the van der Waals surfaces of the full molecules in the same orientation as the stick figures, with red representing positive electrostatic potential and blue for negative potential. The net charge of −1 for methyl thiolate makes the whole assembly more negative, as indicated by the blue color. However, the relative charge distribution shows that the most positive part of the molecule (green) remains the oxocarbenium ion-like ribose ring. Calculations were done with Gaussian 94 at the RHF/6-31G** level. Molecular surfaces are at an electron density of 0.002 e/bohr^3, near the van der Waals surface, and the electrostatic potential spectrum is from −0.1 (blue) to 0.1 hartree/e (red).

more concerted than hydrolysis, it still has substantial oxocarbenium ion character at the transition state. The sum of the bond orders to nicotinamide and Cys351 at the transition state is only 0.20, much less than the C1′−N1 ribosidic bond order of 0.77 in NAD^+. The positive charge from the nicotinamide of reactant NAD^+ is redistributed into the ribosyl ring of the transition state. This charge redistribution may be exploited by the enzyme to stabilize the transition state and thus promote catalysis. The Glu129 side chain is essential for catalysis by pertussis toxin and is invariant for bacterial ADP-ribosylating toxins (*31, 53*). The homologous glutamates have been shown to be essential to the catalytic activities of diphtheria, cholera and *E. coli* exotoxins. In the structure of the transition state docked with the crystal structure of pertussis toxin (Figure 7), the negatively charged carboxyl is positioned to interact with the positive charge on the ribosyl ring at the transition state.

Unlike the well-organized catalytic site of diphtheria toxin (*40*), the binding site for the nicotinamide ring is more open and less well-defined on pertussis toxin. The nicotinamide ring makes contact with residues Ser52, Thr53, Ser5, Gln127, Glu129, and Tyr130. Changes in side chain torsional angles of Tyr59 and Tyr63 could also allow these residues to make contact with the nicotinamide ring. In the X-ray crystal structure, the active-site cleft is part of the interior of the protein, and was exposed by deleting 46 amino acid residues. It would be expected that many side-chain adjustments could occur in solution before NAD^+ binding.

Other residues are also important for ADP-ribosylation including Arg9, His35, and Trp26. In the docked model, Arg9 and His35 are in contact with the pyrophosphate moiety of NAD^+. At high pH, deprotonation of His35 would mean loss of the favorable electrostatic interaction. The expected decrease in rate is observed in pH studies (*54*). The fluorescence from Trp26 is quenched upon NAD^+ binding. In the docked model, it makes contact with the adenylyl ribose ring of NAD^+. Rotation by 180° about $\chi2$ (the Cβ-Cγ bond of Trp26) would bring it into contact with the adenyl ring, consistent with the observed fluorescence quenching.

Docked Model of the Ternary Pertussis Toxin·NAD^+·$G_{i\alpha1}$ Transition-State Complex. With a model of the binary complex of the transition-state structure docked with pertussis toxin, it became possible to examine features of the binding of the ADP-ribose acceptor, $G_{i\alpha1}$. The ADP-ribose acceptor is Sγ of Cys351, four residues from the C-terminal Phe354. Two X-ray crystallographic structures of $G_{i\alpha1}$ have been reported. In the structure complexed with a nonhydrolyzable GTP analogue, GTPγS (guanosine 5′-O-3-thiotriphosphate) (*42*), the C-terminal 11 residues were disordered, with no interpretable electron density. In the structure complexed with GDP (*15*) those residues had interpretable electron density, but the side chain of Cys 351 faces the core of the

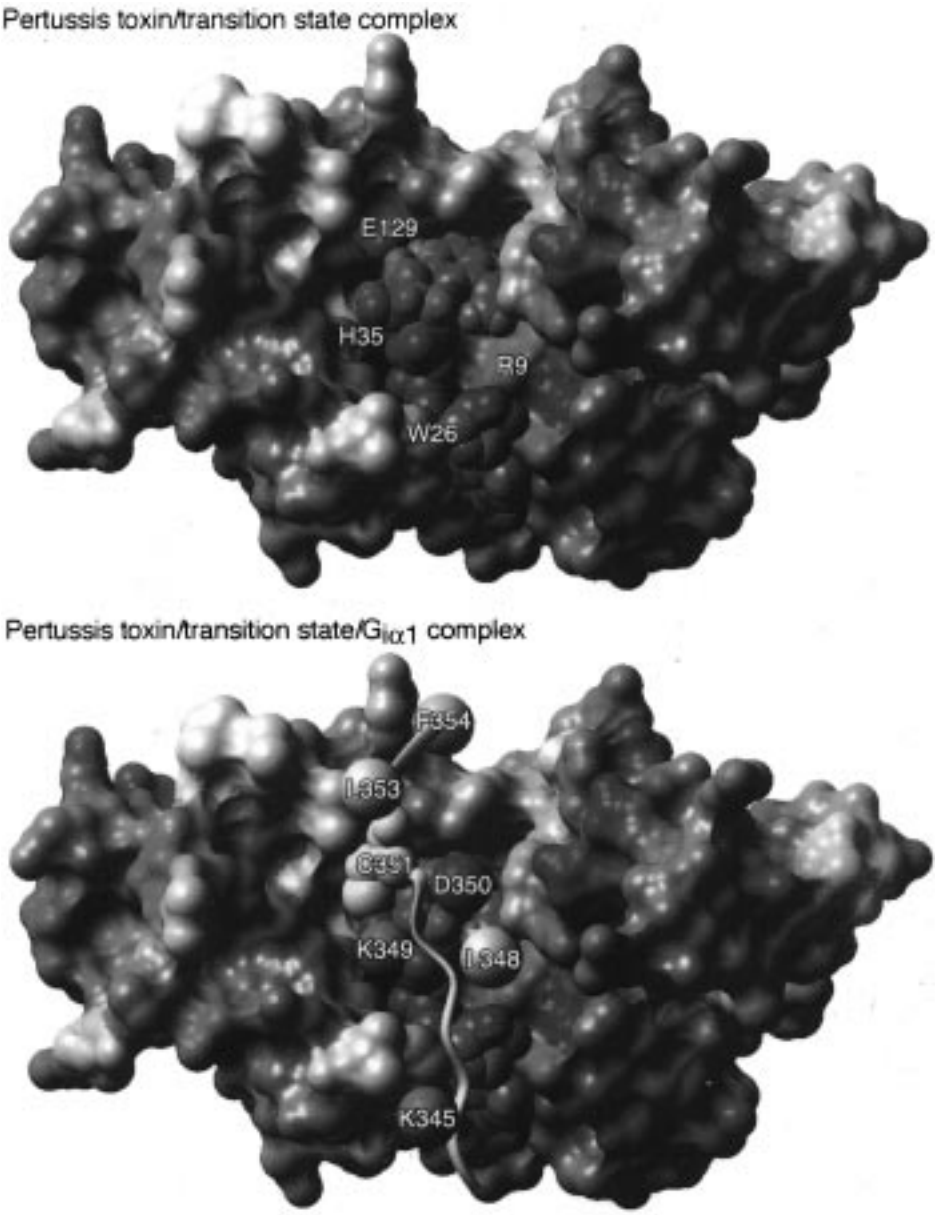

FIGURE 7: Binary complex of pertussis toxin and the NAD^+ transition state. (Top panel) Projection of the electrostatic potentials onto the molecular surface shows the complementarity of the active site for the transition state, with positive potential in red, and negative in blue. The transition state is shown with electroneutral regions in green. Pertussis toxin has the neutral regions in beige (Trp, Tyr, Phe), white (Ile, Leu, Met, Val), or gray (all others). The region of positive potential (red) associated with C1′ of the transition state is apposed with the negative potential (blue) of the carboxylate of Glu129 (E129). Other residues important to catalysis are also labeled: His35 (H35), Arg9 (R9), and Trp26 (W26). (Bottom panel) Ternary complex of pertussis toxin, the transition-state structure of NAD^+ with the $G_{i\alpha1}$ peptide. The yellow ribbon traces the peptide backbone of $G_{i\alpha1}$. The ADP-ribose acceptor, Cys351 is shown. The positions of other side chains are shown schematically with spheres at the position of Cβ. Side chains shown are Lys345, Leu348, Lys349, Asp350, Cys351, Leu353, and Phe354. The protein electrostatic potentials were calculated using the Delphi module of the program Insight II (Biosym Technologies, San Diego, CA). Charges were of +1 were assigned to Lys and Arg residues, +0.5 to His, and −1 to Glu and Asp. Point charges on the atoms of the transition-state structure were assigned from the natural population analysis charges calculated from the structures in Figure 6. The molecular surfaces were calculated as the Connolly surface, but with the atomic radii reduced by a factor of 0.8 so that the surface approximates a smoothed van der Waals surface.

protein, away from the solvent. It is in a conformation in which it could not react with NAD^+.

ADP-ribosylation of $G_{i\alpha1}$ occurs at the same rate in the presence of GTPγS or GDP with only a 2-fold difference in K_m. The solution structure of the C-terminal region which contains the susceptible Cys therefore remains accessible to pertussis toxin in the presence of GDP. The C-terminal peptide from the crystal structure could not be docked into the active-site cleft of the pertussis toxin·NAD^+ binary complex of the transition state without significant steric clashes. Therefore, the peptide was docked in a fully extended conformation. The shape of the active-site cleft of pertussis toxin suggests that the $G_{i\alpha1}$ peptide binds roughly parallel to NAD^+. In this geometry, the position of Cys351 Sγ was in the correct position for nucleophilic attack on the transition-state structure, and the rest of the peptide was positioned to avoid steric clashes. It was necessary to alter backbone ϕ and ψ angles at residues 351 and 352. Docking the peptide in an orientation antiparallel to that shown in Figure 7 offered fewer favorable interactions, and resulted

in the hydrophobic resides Leu353 and Phe354 being in a highly polar part of the active-site cleft near the pyrophosphate of NAD^+.

With the C-terminal peptide docked with the binary pertussis toxin•transition-state complex, Sγ of Cys351 is located directly above the cationic ribose ring of the transition-state structure. The solvent deuterium isotope effect indicates that the nucleophile at the transition state is the thiolate anion of Cys351. There is no obvious candidate in the docked model for a general base catalyst that could abstract the proton from Cys351 Sγ-H. However, it is probable that no general base catalyst is necessary. Given the $\sim 5 \times 10^9$-fold higher nucleophilicity of thiolate anion over a thiol (*55*) and that the reactions were conducted at pH 8.0, where a significant fraction of thiols would be deprotonated, the reaction would be expected to involve a thiolate anion even in the absence of a general base catalyst.

The side chain of Phe354, which is essential for ADP-ribosylation, is located near residues Try59 and Tyr126 of pertussis toxin, where it could form aromatic−aromatic interactions. Leu353 could form hydrophobic interactions with Leu123. Lys349 is located near the pyrophosphate moiety of NAD^+, where it could form favorable ion pair interactions. Leu348 could form hydrophobic interactions with Tyr63 and/or Tyr10. N-terminal to residue 348, the active-site cleft of pertussis toxin becomes wider, and a large number of favorable interactions with $G_{i\alpha1}$ are possible.

Accuracy of the Docked Models. This docking experiment represents a working model of the pertussis toxin•NAD^+•$G_{i\alpha1}$ ternary transition-state complex. Reduction of the Cys41-Cys201 disulfide bond and movement of the C-terminal peptide out of the active-site cleft would be expected to result in adjustments to the active-site amino acids. The overall orientation of the NAD^+ transition state in the active site was guided by using the crystal structure of substrate NAD^+ bound to diphtheria toxin, on which the pertussis toxin molecule was superimposed. The high complementarity of NAD^+ from the superimposed structure of diphtheria toxin with the active site of pertussis toxin indicates similar binding contacts. The docked transition-state structure (a) was close in space to the nicotinamide portion of docked NAD^+, (b) formed favorable interactions with active site residues, and (c) was readily merged with the adenosyl portion of NAD^+. The number of favorable interactions formed in the docked binary complex and the agreement between the docked model and the results of mutagenesis experiments suggest that the proposed binary complex is reasonable.

Neither of the X-ray crystallographic structures of $G_{i\alpha1}$ provided a usable model of the C-terminal peptide, so only general conclusions about its binding may be drawn from the model of the ternary complex. The position of Cys351 is dictated by its orientation relative to the anomeric carbon of the NAD^+ transition state. Potential favorable interactions with the binary complex in the current model suggest that this represents the general binding mode of the $G_{i\alpha1}$ peptide.

Significance of the Pertussis Transition State. The results demonstrate the feasibility of obtaining transition-state structures based on kinetic isotope effect studies for covalent modification of proteins. The ADP-ribose transfer to a variety of acceptor proteins is important for bacterial toxins, DNA repair, and to cellular regulatory functions. The conditions used here represent a simplified system of biological ADP-ribosylation, by the use of high concentrations of isolated α-subunits. Kinetic data with $\alpha\beta\gamma$ trimer give evidence that the differences are mainly due to the affinity of the complete trimer and the isolated α-subunit to the toxin. The catalytic rates obtained at saturating concentrations of α-subunits are in the same range as those obtained in the presence of $\beta\gamma$-subunits.

The development of transition-state inhibitors for pertussis toxin may be possible based on the transition state of ADP-ribosylation of $G_{i\alpha1}$. Incorporation of an analogue of the C-terminal portion of α-subunits may result in an additional increase of affinity. However, experiments with phenyliminoribitol nucleoside analogues, which have been shown to be potent inhibitors for other ribohydrolases, showed no significant inhibition for the ADP ribosylation of $G_{i\alpha1}$ subunit by pertussis toxin. Introduction of the ADP-moiety to provide a transition state analogous to the oxocarbenium ion of NAD^+ may provide the necessary contacts to the binding site of pertussis toxin. Exploration of these chemistries is now underway for the development of transition-state inhibitors for ADP-ribosylation reactions.

REFERENCES

1. Domenighini, M., Pizza, M., and Rappuoli, R. (1995) in *Handbook of Natural Toxins* (Moss, J., Inglenski, B., Vaughan, M., and Tu, A., Eds.) Vol. 8, Bacterial Toxins and Virulence Factors in Disease, pp 59−80, Dekker, Inc., New York.
2. Moss J., and Vaughan, M. (1988) *Adv. Enzymol. 61*, 303−379.
3. Hepler, J. R., and Gilman, A. G. (1992) *Science 17*, 383−387.
4. Gilman, A. G. (1987) *Annu. Rev. Biochem. 56*, 615−649.
5. Katada, T., and Ui, M. (1982) *Proc. Natl. Acad. Sci. U.S.A 79*, 3129−3133.
6. West, R. E. Jr., Moss, J., Vaughan, M., Liu, T. and Liu, T.Y (1985) *J. Biol. Chem. 260*, 14428−14430.
7. Katada, T., Iiri, T., Takahashi, K., Nishina, H., and Kanaho, Y. (1995). *Handbook of Natural Toxins* (Moss, J., Inglenski, B., Vaughan, M., and Tu, A., Eds.) Vol. 8, Bacterial Toxins and Virulence Factors in Disease, pp 459−489, Dekker, Inc., New York.
8. Ui, M. (1984) *Trends Pharmacol. Sci. 5*, 277−279.
9. Casey, P. J., Graziano, M. P., and Gilman, A. G. (1989) *Biochemistry 28*, 611−616.
10. McDonald, L., Wainschel, L. A., Oppenheimer, N. J., and Moss, J. (1992) *Biochemistry 31*, 11881−11889.
11. Moss, J., and Vaughan, M. (1977) *J. Biol. Chem. 252*, 2455−2457.
12. Graf, R., Codina, J., and Birnbaumer, L. (1992) *Mol. Pharmacol. 42*, 760−764.
13. Finck-Barbancon, V., and Barbieri, J. T. (1995) *Biochemistry 34*, 1070−1075.
14. Scheuring J., and Schramm, V. L. (1995) *J. Am. Chem. Soc. 117*, 12652−12654.
15. Mixon, M. B., Lee, E., Coleman, D. E., Berghuis, A. M., Gilman, A. G., and Sprang, S. R. (1995) *Science 270*, 954−960.
16. Stein, P. E., Boodhoo, A., Armstrong, G. D., Cockle, S. A., Klein, M. H., and Read, R. J. (1994) *Structure 2*, 45−57.
17. Northrup, D. (1981) *Annu. Rev. Biochem. 50*, 103−131.
18. Mentch, F., Parkin, D. W., and Schramm, V. L. (1987) *Biochemistry 26*, 921−930.
19. Parkin, D. W., Mentch, F., Banks, G. A., Horenstein, B. A., and Schramm, V. L. (1991) *Biochemistry 30*, 4586−4594.
20. Horenstein, B. A., Parkin, D. W., Estupinan, B., and Schramm, V. L. (1991) *Biochemistry 30*, 10788−10795.
21. Kline, P. C., and Schramm, V. L. (1993) *Biochemistry 32*, 13212−13219.

22. Rising, K. A., and Schramm, V. L. (1997) *J. Am. Chem. Soc. 119*, 27−37.
23. Berti, P. J., Blanke, S. R., and Schramm, V. L. (1997) *J. Am. Chem. Soc. 119*, 12079−12088.
24. Horenstein, B. A., and Schramm, V. L. (1993) *Biochemistry 32*, 9917−9925.
25. Boutellier, M., Horenstein, B. A., Semenyaka, A., Schramm, V. L., and Ganem, B. (1994) *Biochemistry 33*, 3994−4000.
26. Parkin, D. W., Limberg, G., Tyler, P. C., Furneaux, R. H., Chen, X.-Y., and Schramm, V. L. (1997) *Biochemistry 36*, 3528−3534.
27. Furneaux, R. H., Limberg, G., Tyler, P. C., and Schramm, V. L. (1997) *Tetrahedron 53*, 2915−2930.
28. Scheuring, J., and Schramm, V. L. (1997) *Biochemistry 36*, 4526−4534.
29. Scheuring, J., and Schramm, V. L. (1997) *Biochemistry 36*, 8215−8223.
30. Lee, E., Linder, M. E., and Gilman, A. G. (1994) *Methods Enzymol. 237*, 146−164.
31. Burns, D. L. (1995) *Handbook of Natural Toxins* (Moss, J., Inglenski, B., Vaughan, M., and Tu, A., Eds.) Vol. 8, Bacterial Toxins and virulence Factors in Disease. pp 441−458, Dekker, New York.
32. Rising, K. A., and Schramm, V. L. (1994) *J. Am. Chem. Soc. 116*, 6531−6536.
33. Sternweis, P. C., and Robishaw, J. D. (1984) *J. Biol. Chem. 259*, 13806−13813.
34. Parkin, D. W. (1991) in *Enzyme Mechanism from Isotope Effects* (Cook, P. F., Ed.) pp 269−290, CRC Press, Boca Raton, FL.
35. Berti, P. J., and Schramm, V. L. (1997) *J. Am. Chem. Soc. 119*, 12069−12078.
36. Sims, L. B., Burton, G. W., and Lewis, D. E. (1977) BEBOVIB−IV, Quantum Chemistry Program Exchange, No. 337, Indiana University, Bloomington, IN.
37. Bigeleisen, J., and Wolfsberg, M. (1958) *Adv. Chem. Phys. 1*, 15−76.
38. Moss, J., Stanley, S. J., Burns, D. L., Hsia, J. A., Yosts, D. A., Myers, G. A., and Hewlett, E. L. (1983) *J. Biol. Chem. 258*, 11879−11882.
39. Cortina, G., Krueger, K. M., and Barbieri, J. T. (1991) *J. Biol. Chem. 266*, 23810−23814.
40. Bell, C. E., and Eisenberg, D. (1996) *Biochemistry 35*, 1137−1149.
41. Reeck, G. R., deHaen, C., Teller, D. C., Doolittle, R. F., Fitch, W. M., Dickerson, R. E., Chambon, P., Machachlan, A. D., Margoliash, E., Jukes, T. H., and Zuckerkandl, E. (1987) *Cell 50*, 667−670.
42. Coleman, D. E., Berghuis, A. M., Lee, E., Linder, M. G., Gilman, A. G., and Sprang, S. R. (1994) *Science 265*, 1405−1412.
43. Rose, I. A. (1980) *Methods Enzymol. 64, 47−83.*
44. Quinn, D. M., and Sutton, L. D. (1991) in *Enzyme Mechanism From Isotope Effects* (Cook, P. F., Ed.) pp 73−126, CRC Press, Boca Raton, FL.
45. Westaway, K. C. (1975) *Tetrahedron Lett. 48*, 4229−4232.
46. Westaway, K. C., and Ali, S. F. (1979) *Can J. Chem. 57*, 1354−1367.
47. Westaway, K. C. (1993) *Can. J. Chem. 71*, 2084−2094.
48. Westaway, K. C., VanPham, T, and Fang, Y. R. (1997) *J. Am. Chem. Soc. 119*, 3670−3676.
49. Bennet, A. J., and Sinnott, M. L. (1986) *J. Am. Chem. Soc. 108*, 7287−7294.
50. Glad, S. S., and Jensen, F. (1997) *J. Am. Chem. Soc. 119*, 227−232.
51. Barnes, J. A., and Williams, I. H. (1993) *J. Chem. Soc., Chem. Commun*. 1286−1287.
52. Poirier, R. A., Wang, Y., and Westaway, K. C. (1994). *J. Am. Chem. Soc. 116*, 2526−2533.
53. Avigan, J., Murtagh, J. J., Jr., Stevens, L. A., Angus, C. W., Moss, J., and Vaughn, M. (1992) *Biochemistry 31*, 7736−7740.
54. Antoine, R., and Locht, C. (1994) *J. Biol. Chem. 269*, 6450−6457.
55. Roberts, D. D. Lewis, S. D., Ballou, D. P., Olson, S. T., and Shafer, J. A. (1986) *Biochemistry 25*, 5595−5601.
56. Huskey, W. P. (1991) In *Enzyme Mechanism from Isotope Effects* (Cook, P. F., Ed.) pp 37−72, CRC Press, Boca Raton, FL.
57. Sims, L. B., and Lewis, D. E. (1984) In *Isotopes in Organic Chemistry* (Buncel, E., and Lee, C. C., Eds.) pp 161−259, Elsevier, New York.

BI972594X